HiSST: 2nd International Conference on
High-Speed Vehicle Science Technology
11–15 September 2022, Bruges, Belgium

Practical Adaptive Notch Filter Design for Aeroservoelasticity Suppression of High-Speed Vehicle

Minnan Piao[1], Zhigang Chen[2], Mingwei Sun[3], Xinhua Zhang[4], Zengqiang Chen[3]*

Abstract

In this paper, an adaptive notch filter (ANF) design approach is proposed for the flexible high-speed vehicle. For practical applications, the requirements for the ANF are analyzed first, among which the direct acquisition of the frequency estimation is particularly important for the online effectiveness monitoring. Thus, two schemes for the direct frequency estimation, the individual adaptation (IA) and the simultaneous adaptation (SA) based on the recursive maximum likelihood method, respectively, are comprehensively compared. To guarantee that all the frequencies can be estimated precisely under the low signal-to-noise ratio, a strategy of supervising the frequency estimations is proposed for the two schemes. It is concluded that the convergence performance can be improved significantly with such a strategy. Moreover, it is found that the estimation bias of the supervised SA (SSA) is smaller than that of the supervised IA (SIA) both in tracking stationary and time-varying frequencies. Thus, the SSA method is more favourable in practice due to the high precision and robustness. Finally, simulations on a flexible high-speed vehicle are performed to demonstrate the effectiveness of the proposed SSA in the aeroservoelasticity suppression.

Keywords: Flexible high-speed vehicle, aeroservoelasticity suppression, practical adaptive notch filter, multiple structural modes, direct frequency estimation

1. Introduction

In recent years, there has been a growing research effort devoted to the high-speed vehicle (HSV). The HSV is characteristic of a slender airframe and lightweight materials. Thus, the HSV cannot be regarded as a rigid-body and the bending vibration must be taken into account. In this paper, we mainly focus on the control problem brought by the flexible vibration. The vibration can cause the thrust and aerodynamic force perturbations. Moreover, the flexible deformation sensed by the rate gyros or accelerometers can be introduced into the flight control loop, which can affect the stabilities of the structural modes. These two effects together formulate the aeroservoelasticity (ASE) problem which has been a main concern in the aerospace industry. However, the investigations for the ASE suppression of the HSV are deficient and only the aeroelastic effect is considered in most of the present literature [1].

For the HSV, the frequencies of the structural modes are time-varying due to the fuel consumption and aerodynamic heating, and the variation range may be large due to the wide flight envelope. Moreover, the frequency of the low-order structural mode is relatively low compared with that of the rigid-body and thus the coupling between the rigid-body and structural dynamics is strong. To guarantee the precision of attitude control and the proper operation of the scramjet engine, a reliable ASE suppression scheme which can deal with the time-varying frequencies without degrading the control performance of the rigid-body is urgently needed in practice. Adaptive notch filter (ANF) is an effective and popular approach for estimations of sinusoidal frequencies and has been a major research problem in the signal processing field. ANF has been used widely in the areas of communication, sonar, radar, and biomedical,

[1] *College of Computer Science and Technology, Civil Aviation University of China, Tianjin, China, mnpiao@cauc.edu.cn*
[2] *Science and Technology on Space Physics Laboratory, Beijing, China, czg1983914@163.com*
[3] *College of Artificial Intelligence, Nankai University, Tianjin, China, smw_sunmingwei@163.com, chenzq@nankai.edu.cn*
[4] *Beijing Institute of Automatic Control Equipment, Beijing, China, sloht0033@126.com*

while the investigations of its application in the ASE problem are still relatively few and more efforts on how to solve the ASE problem better by using the excellent work in the ANF area are needed. Based on the characteristics of the ASE suppression, the following problems should be solved by the ANF:

- The only need for the algorithm should be the rate gyro measurement. In [2], the rigid-body dynamics is also needed for frequency identification, which is impractical since the precise model of the rigid-body dynamics cannot be obtained.
- The estimation bias should be as small as possible to effectively filter out the vibration components in the measurement.
- The direct acquisitions of frequency estimations are required so as to perform the online supervision. We must judge online whether the frequency estimations are physically reasonable or not since all the adaptation algorithms are stochastic to a certain degree and the frequency estimations cannot be ensured to converge to the proper values. If the frequency estimation wrongly converges to a local minimum that is very close to the rigid-body frequency, the stability of the entire closed-loop may be violated. Thus, this property is pretty important for the consideration of reliability.
- The simultaneous suppressions of multiple structural modes whose frequencies or power may be close to each other can be achieved.
- The effectiveness of the algorithm under the low signal-to-noise ratio (SNR) scenario should be guaranteed. This condition generally happens when the frequency estimation is close to its true value and the energy of the structural mode is relatively weak.
- The algorithm should be robust to the finite wordlength. In practice, the ANF is implemented in the processor like the digital signal processor (DSP), and the calculation precision is finite. The finite wordlength may cause the instability of the filter and make the actual zeros be not on the unite circle.
- The algorithm should be insensitive to the changes of the sinusoidal amplitudes. The strength of each structural mode changes during the flight, and the adaptation algorithm with the fixed design parameters should guarantee that the estimations can converge to the true values in spite of the energy variation.

There are two schemes to realize the frequency estimation, the indirect approach and the direct approach, respectively, according to whether the factorization is needed. The former estimates the polynomial coefficients first and then calculates the frequencies via the factorization. For high-order polynomials (higher than two orders), the factorization is computationally complicated. In addition, the calculated frequencies are sensitive to the polynomial coefficients and small perturbations can make the frequencies shift remarkably. Thus, the direct approach is more favorable for the ASE problem. The direct approach can be realized through two different ways, the individual adaptation (IA) and the simultaneous adaptation (SA) [3]. The differences between these two schemes are shown in Fig. 1. In the IA scheme, the ANF can be regarded as the series connections of many second-order ANFs and the parameters of each ANF are adapted individually based on the local input and output data. All the aforementioned identification algorithms can be applied in this scheme and the recursive maximum likelihood (RML) is expected to yield the best results. For the SA scheme, all the parameters of the ANF are adapted simultaneously based on one error signal. In [4] and [3, 5], two different approaches were proposed under the SA scheme. In [4], the frequency estimations have to be converted to the polynomial coefficients to calculate the prediction error and the error gradient. Since the ANF algorithm needs to be implemented in the processor of finite wordlength in practice, this conversion may cause the violation of the stability that is guaranteed under the infinite precision. Different from [4], the polynomial coefficients are not required for the update and the frequencies are the only parameters of the ANF [3, 5]. In this way, the robustness to the finite precision can be improved. The approximate maximum likelihood (AML) and RML methods were employed in [3] and [5], respectively, and the RML method in this scheme can have better performances just as in the IA scheme. Based on the above literature research and analysis, it can be known that the RML algorithm performed under the IA and the SA schemes can provide a promising solution to the ASE suppression problem in our paper. One intuitive and critical question emerges that whether the IA scheme or the SA scheme can achieve better performance against our aforementioned problems. Thus, in this paper, we perform a comprehensive

comparison between the IA and the SA schemes with the RML as the identification algorithm. To guarantee that all the frequencies can be estimated precisely under the low SNRs and other disturbances, a strategy of adding constraints on the frequency estimations is proposed for the two schemes and it is concluded that the convergence performance can be improved remarkably. Moreover, it is found that the estimation bias of the supervised SA (SSA) scheme is smaller than that of the supervised IA (SIA) both in tracking stationary and time-varying frequencies. Thus, the SSA method is more favourable in practice due to the high precision and robustness.

The remainder of the paper is organized as follows. The flexible HSV model and the corresponding control problem are formulated in Section 2. The attitude control law design is briefly introduced in Section 3. Design and comparisons of two types of ANFs are presented in Section 4. The simulation results on a flexible HSV model are provided in Section 5. Finally, concluding remarks are given in Section 6.

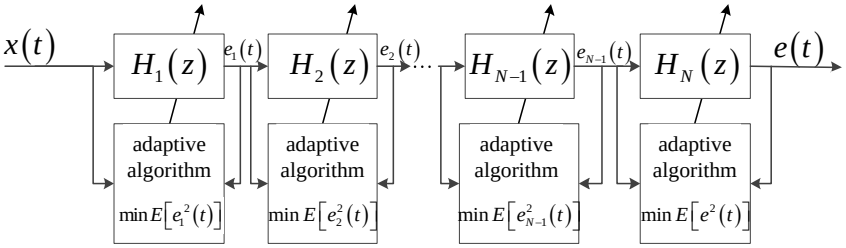

(a) IA scheme

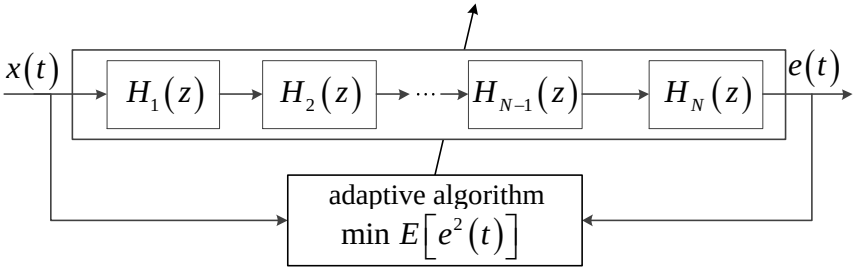

(b) SA scheme

Fig. 1 Two schemes for the direct estimations of frequencies, where $H_i(z)$ represents the i[th] second-order adaptive notch filter.

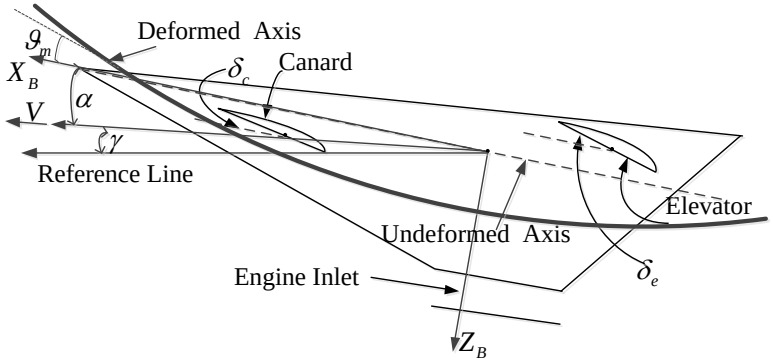

Fig. 2 Geometry of the flexible HSV.

2. Problem formulation

The HSV studied in this paper is taken from the curve-fitted model derived by [6], wherein the intricate interactions among the propulsion system, aerodynamics, and the vibration dynamics are captured. The geometry of the flexible HSV is shown in Fig. 2. In this model, the thrust, lift, drag, and the moment

coefficients depend explicitly on the elastic modes, which reflects the aeroelastic effect. The rate gyro is employed to measure the pitch angular rate for the pitch angle control. Due to the flexible deformation, the rate gyro measures not only the rigid-body pitch angular rate but also the flexible pitch angular rate at the sensor position as shown in Fig. 2. After the vibration modeling, we can obtain the measurements of the pitch angle and pitch angular rate as

$$\begin{aligned} Q_m &= Q - \sum_{i=1}^{3} \frac{\mathrm{d}\,\phi_i\left(x_{\mathrm{rg}}\right)}{\mathrm{d}\,x}\dot{\eta}_i \\ \vartheta_m &= \vartheta - \sum_{i=1}^{3} \frac{\mathrm{d}\,\phi_i\left(x_{\mathrm{rg}}\right)}{\mathrm{d}\,x}\eta_i \end{aligned} \tag{1}$$

Readers can refer to [1, 6] for the modeling process and the values of the model parameters. Only three structural modes are considered in this model and it is assumed that all the three structural modes are suppressed by the ANF in this paper. Q_f is the only available signal for the ANF design. The function of the ANF is to effectively filter out the flexible components in the measurement so as to achieve the gain stabilization of the flexible modes.

3. Attitude control design

Linear active disturbance rejection control (LADRC) [7] is employed in this paper for the attitude control to deal with the strong coupling effects and uncertainties of the HSV model. Details of the design process are not interpreted since it is not the emphasis of this paper. The readers interested in the application of LADRC to the HSV control can refer to [1, 8].

4. Adaptive notch filter design and comparisons

In this section, two types of ANFs, based on the IA and SA schemes, respectively, are designed and compared. The ANF model is selected as the constrained pole-zero notch filter [9]

$$H\left(z^{-1}\right) = \frac{A\left(z^{-1}\right)}{A\left(\rho z^{-1}\right)} = \prod_{i=1}^{N} \frac{1 - 2\cos\theta_i z^{-1} + z^{-2}}{1 - 2\cos\theta_i \rho z^{-1} + \rho^2 z^{-2}} \tag{2}$$

Next, two types of ANFs are designed based on (2) and the RML algorithm.

4.1. IA design

In [10], comparisons of the stochastic Gauss-Newton (SGN), RML, AML, and the AGB (Approximate Gradient Based) were performed and it was concluded that the RML yields the best result. In recent years, the SM algorithm becomes another effective adaptive algorithm for the ANF design. Thus, we also performed the ANF design with the SM method under the IA scheme to compare its performance with the RML. The simulation results showed that the estimation bias of the SM is much larger than that of the RML (The simulation results are not presented due to the space limit). Thus, the RML is the best method suitable for the IA design according to the author's knowledge. The cost function to be optimized for each ANF is

$$V_i = \frac{1}{N_s}\sum_{k=1}^{N_s} \lambda^{k-1} e_i^{\,2}(k) \tag{3}$$

The RML algorithm under the IA scheme can be summarized as follows [4]:
Step 1: prediction error calculation

$$\begin{aligned} &e_i(k) = x_i(k) + x_i(k-2) - \rho^2(k)\bar{e}_i(k-2) - a_i(k-1)\left(\rho(k)\bar{e}_i(k-1) - x_i(k-1)\right) \\ &x_1(k) = x(k),\ x_i(k) = \bar{e}_{i-1}(k),\ i = 2,3,\cdots N \end{aligned} \tag{4}$$

Step 2: gradient calculation

$$\psi_i(k) = -a_i(k-1)\rho(k)\psi_i(k-1) - \rho^2(k)\psi_i(k-2) + \left(\rho(k)\bar{e}_i(k-1) - x_i(k-1)\right) \tag{5}$$

Step 3: parameter update

$$P_i(k)=\frac{1}{\lambda(k)}\left[P_i(k-1)-P_i(k-1)\psi_i(k)\psi_i^T(k)P_i(k-1)\Big/\left(\lambda(k)+\psi_i^T(k)P_i(k-1)\psi_i(k)\right)\right] \tag{6}$$

$$a_i(k)=a_i(k-1)+P_i(k)\psi_i(k)e_i(k) \tag{7}$$

Step 4: calculation of posteriori prediction error

$$\begin{aligned}&\bar{e}_i(k)=x_i(k)+x_i(k-2)-\rho^2(k)\bar{e}_i(k-2)-a_i(k)\left(\rho(k)\bar{e}_i(k-1)-x_i(k-1)\right)\\&x_1(k)=x(k),\ x_i(k)=\bar{e}_{i-1}(k),i=2,3,\cdots N\end{aligned} \tag{8}$$

Step 5: update of design parameters

$$\begin{aligned}&\rho(k+1)=\rho_w\rho(k)+(1-\rho_w)\rho_s\\&\lambda(k+1)=\lambda_w\lambda(k)+(1-\lambda_w)\lambda_s\end{aligned} \tag{9}$$

Step 6: frequency calculation

$$\omega_i(k)=\arccos\left(-a_i(k)/2\right)/t_s \tag{10}$$

Some remarks are given for this algorithm. First, stability monitoring is necessary since a_i is the direct estimation parameter and its range should be $|a_i(k)|\le 2$. The stability projection

$$\text{sat}\left(a_i(k),2\right)=\begin{cases}a_i(k), & |a_i(k)|<2\\ 2\text{sign}\left(a_i(k)\right), & |a_i(k)|\ge 2\end{cases} \tag{11}$$

should be performed to guarantee the stability. Second, the posteriori prediction error $\bar{e}_i(k)$ instead of the priori error $e_i(k)$ is used in (4) and (5) since this can improve the convergent rate, and it is the only difference between the RML and SGN methods. In the SGN method, $e_i(k)$ is used both in the error prediction and gradient calculation.

4.2. SA design

The RML algorithm under the SA scheme can be summarized as follows [5]:

Step 1: prediction error calculation

$$\begin{aligned}&e_i(k)=2\cos\theta_i(k-1)\left(\rho(k)-\sigma\right)Z_i\ (k-1)+\left(\sigma^2-\rho^2(k)\right)Z_i\ (k-2)+x_i(k)\\&x_1(k)=x(k),\ x_i(k)=e_{i-1}(k),\ i=2,3,\cdots N,\ e(k)=e_N(k)\end{aligned} \tag{12}$$

Step 2: gradient calculation

$$\begin{aligned}&e_{Fi}(\sigma,k)=2\sigma\cos\theta_i(k-1)e_{Fi}(\sigma,k-1)-\sigma^2e_{Fi}(\sigma,k-2)+\sigma\bar{e}_N(k-1)\\&e_{Fi}(\rho,k)=2\rho(k)\cos\theta_i(k-1)e_{Fi}(\rho,k-1)-\rho^2(k)e_{Fi}(\rho,k-2)+\rho(k)\bar{e}_N(k-1)\\&\psi_i(k)=-2\sin\left[\theta_i(k-1)\right]\left(e_{Fi}(\sigma,k)-e_{Fi}(\rho,k)\right)\\&\boldsymbol{\psi}(k)=\left[\psi_1(k),\psi_2(k),\cdots,\psi_N(k)\right]^T\end{aligned} \tag{13}$$

Step 3: parameter update

$$\boldsymbol{P}(k)=\frac{1}{\lambda(k)}\left[\boldsymbol{P}(k-1)-\boldsymbol{P}(k-1)\boldsymbol{\psi}(k)\boldsymbol{\psi}^T(k)\boldsymbol{P}(k-1)\Big/\left(\lambda(k)+\boldsymbol{\psi}^T(k)\boldsymbol{P}(k-1)\boldsymbol{\psi}(k)\right)\right] \tag{14}$$

$$\boldsymbol{\theta}(k)=\boldsymbol{\theta}(k-1)+\boldsymbol{P}(k)\boldsymbol{\psi}(k)e(k) \tag{15}$$

Step 4: posteriori prediction error calculation

$$\begin{aligned}&\bar{e}_i(k)=2\cos\theta_i(k)\left(\rho(k)-\sigma\right)Z_i\ (k-1)+\left(\sigma^2-\rho^2(k)\right)Z_i\ (k-2)+\bar{e}_{i-1}(k)\\&Z_i\ (k)=2\rho(k)\cos\theta_i(k)Z_i\ (k-1)-\rho^2(k)Z_i\ (k-2)+\bar{e}_{i-1}(k)\\&\bar{e}_0(k)=x(k)\end{aligned} \tag{16}$$

Step 5: update of design parameters

$$\begin{aligned}\rho(k+1)&=\rho_w\rho(k)+(1-\rho_w)\rho_s\\ \lambda(k+1)&=\lambda_w\lambda(k)+(1-\lambda_w)\lambda_s\end{aligned} \tag{17}$$

Stability monitoring is not needed in this algorithm since θ_i is directly estimated and the stability of (2) is always ensured. The adaptation objective of all the frequencies is to minimize the error output $e(t)$, and thus the convergent rate can be faster than that of the IA theoretically.

4.3. Simulation comparisons and online supervision strategy

In the simulation, the input signal includes three sinusoids, and their frequencies are the first three structural frequencies of the HSV. The nominal values of the frequencies at different fuel levels are shown in Table 1. The sampling time t_s is $0.001\,\mathrm{s}$ for all the cases. For each algorithm, these parameters are adjusted to achieve the best performance in each case, and the design parameters are shown in Table. 2. The following three cases are considered:

Case 1: The three sinusoidal signals have the equal power and the input signal is in the form of

$$y(t)=\sin(2\pi\times 3.21t)+\sin(2\pi\times 7.70t)+\sin(2\pi\times 15.22t) \tag{18}$$

The simulation results are shown in Fig. 3. It can be seen that the first two estimations of the IA have faster convergent rate while the third one is much slower. In the steady state, the SA can converge to the true values precisely, while there exist oscillations in the IA method. Although the SA can achieve better performance than the IA for the signal in (18), its performance is quite fragile and sensitive to the values of $\boldsymbol{\theta}(0)$, κ, and amplitudes of the sinusoidal signals.

Case 2: A zero mean white noise process with variance σ^2 is added to (18). SNR is set as 0 dB, 3 dB, 6 dB, and 12 dB. Through simulations, we found that the convergence to the true frequencies cannot be guaranteed in the presence white noise and one or more frequencies will be missed for both schemes. The performance becomes worse when the SNR is very low. To solve this problem, we propose a strategy to improve the convergence performance based on the priori knowledge about the frequency range. Suppose that the range of each structural frequency is known and we have

$$\begin{aligned}&\omega_1^l\le\omega_1\le\omega_1^u,\ \omega_2^l\le\omega_2\le\omega_2^u,\ \omega_3^l\le\omega_3\le\omega_3^u\\ &\omega_1^u<\omega_2^l,\ \omega_2^u<\omega_3^l\end{aligned} \tag{19}$$

where ω_i^l and ω_i^u are the lower and upper bounds of the frequency, respectively. Although the precise value of the structural frequency cannot be obtained, the approximate range can be determined through the CFD analysis and ground vibration test. This range can be made as large as possible to cover the true frequency. However, interactions between the ranges for different frequencies should be avoided so that all the frequencies can be estimated. The strategy is designed as

$$\begin{aligned}&\text{If } \omega_i>\omega_i^u, \text{ then } \omega_i=\omega_i^u\\ &\text{If } \omega_i<\omega_i^l, \text{ then } \omega_i=\omega_i^l\end{aligned} \tag{20}$$

Each section of the ANF is specified to search for the best estimation of one frequency in the corresponding range. With such an improvement, the SSA method becomes more robust to the changes of the initial frequency guesses and the amplitudes. The standard deviations for $\lambda_s=0.997$ are shown in Table 3. (The standard deviation is the average of 100 simulations and the standard deviation for each simulation is calculated with the data of the last two seconds) In general, the estimation precision of the SSA is higher than that of the SIA.

Case 3: In this case, the comparison of tracking time-varying frequencies is conducted. The input signal is in the form of

$$y(t)=\sin\left((10+k_1t)t\right)+\sin\left((40+k_2t)t\right)+\sin\left((80+k_3t)t\right) \tag{21}$$

where $k_1=1$, $k_2=1.5$, and $k_3=6$. Based on the definition of the instantaneous frequency (IF) [12], the IF in the real time should be

$$\omega_1=10+2k_1t,\ \omega_2=40+2k_2t,\ \omega_3=80+2k_3t \tag{22}$$

To track the time-varying frequency, the forgetting factor has to be reduced to 0.996. The simulation results are shown in Fig. 4. It can be seen that both methods can track the trend of the time-varying frequency. The fluctuation of ω_1 under the SIA scheme is stronger than that under the SSA scheme.

The standard derivations of estimation bias for 100 simulations are shown in Table 4. It is evident that the estimation bias is proportional to the change rate of the frequency and the third frequency has the largest bias. In general, the SSA can achieve a higher estimation precision.

Based on the investigations in the above three cases, it can be concluded as follows:

- When there is no noise, the IA outperforms the SA since its performance is not sensitive to the initial guesses of the frequencies and the amplitudes of the sinusoids.
- When the SNR is low, both schemes cannot work well and not all the estimations can converge to the true values. A priori knowledge about the frequency range is required to improve the convergent rate and guarantee all the frequencies can be estimated.
- With the constraint on the frequency estimation, performances of both schemes can be improved significantly and the estimation bias of the SSA scheme is smaller than that of the SIA both in tracking the stationary and time-varying frequencies. Thus, the SSA method is more favorable in practice due to the high precision and robustness.

Table 1. Frequencies for different fuel levels

Fuel level	0%	50%	100%	ω^l	ω^u
ω_1 (rad/s)	22.78	21.17	20.17	10	30
ω_2 (rad/s)	68.94	53.92	48.4	40	70
ω_3 (rad/s)	140	109.1	95.6	80	200

Table 2. Parameters design for the three cases

	IA	SA
Case 1	$\rho(0)=0.9$, $\rho_s=0.995$, $\rho_w=0.99$, $\lambda(0)=0.8$, $\lambda_s=0.999$, $\lambda_w=0.99$, $\kappa=100000$, $\boldsymbol{\theta}(0)=0.5\boldsymbol{\theta}^*$	$\rho(0)=0.8$, $\rho_s=0.995$, $\rho_w=0.99$, $\lambda(0)=0.8$, $\lambda_s=0.999$, $\lambda_w=0.99$, $\kappa=30$, $\boldsymbol{\theta}(0)=0.5\boldsymbol{\theta}^*$
Case 2	$\boldsymbol{\theta}(0)=0.01\boldsymbol{\theta}^*$, $\lambda_s=0.999$, $\lambda_s=0.997$	$\boldsymbol{\theta}(0)=0.01\boldsymbol{\theta}^*$, $\lambda_s=0.999$, $\lambda_s=0.997$
Case 3	$\boldsymbol{\theta}(0)=0.01\boldsymbol{\theta}^*$, $\lambda_s=0.996$	$\boldsymbol{\theta}(0)=0.01\boldsymbol{\theta}^*$, $\lambda_s=0.996$

Table 3. Standard deviation of estimation bias for different SNRs (case 2)

	Standard deviation of estimation bias for IA			Standard deviation of estimation bias for SA		
	ω_1 (rad/s)	ω_2 (rad/s)	ω_3 (rad/s)	ω_1 (rad/s)	ω_2 (rad/s)	ω_3 (rad/s)
0 dB	0.4904	0.2855	0.1460	0.1711	0.1483	0.1448
3 dB	0.4788	0.2658	0.1039	0.1209	0.0979	0.1041
6 dB	0.4715	0.2558	0.0711	0.0835	0.0635	0.0745

Table 4. Standard deviation of estimation bias for different SNRs (case 3)

	Standard deviation of estimation bias for IA			Standard deviation of estimation bias for SA		
	ω_1 (rad/s)	ω_2 (rad/s)	ω_3 (rad/s)	ω_1 (rad/s)	ω_2 (rad/s)	ω_3 (rad/s)
0 dB	0.6683	0.8118	3.1919	0.5470	0.8621	3.0465
3 dB	0.6544	0.7994	3.1167	0.5056	0.8525	3.0125
6 dB	0.6492	0.7929	3.1006	0.4830	0.8483	2.9895

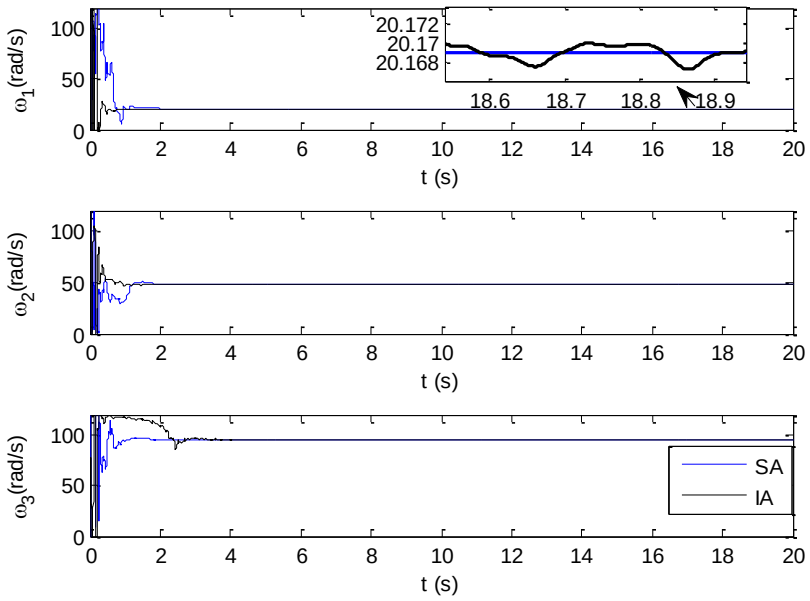

Fig.3 Simulation results for case 1.

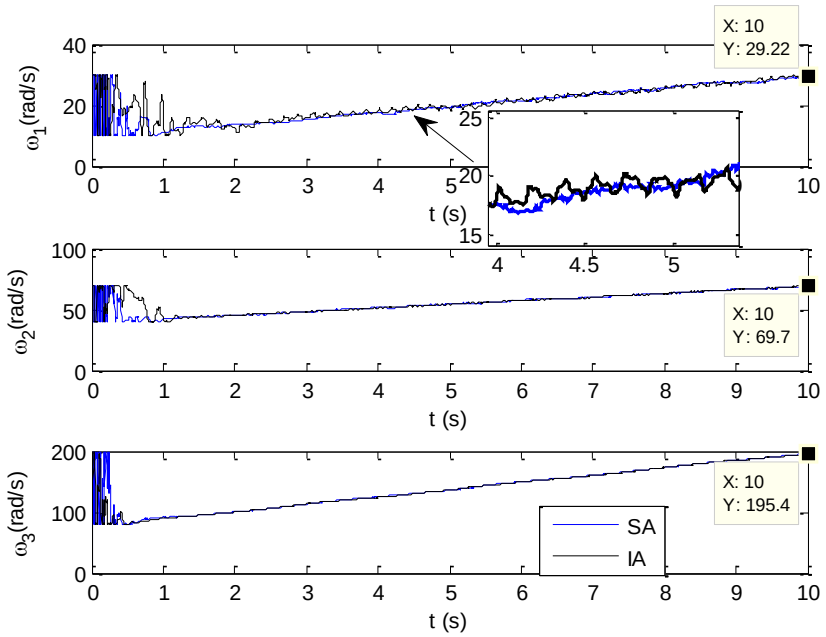

Fig.4 Simulation results for case 3 with SNR=0 (with strategy).

5. Simulation results

In this section, simulations are performed on a flexible HSV model and the proposed SSA method is employed for the ASE suppression. A white noise with the standard deviation of 0.0167 rad/s is added to the measurement of the pitch angular rate. Two rate gyros are needed and the difference of these two measurements is used as the ANF input to eliminate the effect of the rigid-body motion. The parameters of the ANF are the same as these in case 3 in the last section. The simulation results are shown in Figs. 5-7. From the response of the pitch angle in Fig. 5, it can be seen that the structural modes are attenuated gradually and completely suppressed after 50 seconds. The frequency estimations are presented in Fig. 6, and it can be observed that all the frequencies can be tracked

precisely. The measurement of the pitch angular rate and the filtered output is shown in Fig. 7, and it can be seen that only the white noise finally remains in the signal. Note that the frequency estimation of the structural mode is more difficult than the pure sinusoid since the form of the practical signal is more complicated and the energy of the structural mode varies significantly (the relative amount of energy among structural modes also vary during the flight). Thus, the supervision on the frequency estimation is quite necessary. Fig. 8 shows the frequency estimation result when no supervision is added, and it can be seen that only the first frequency is captured correctly and the second frequency is missed all the time.

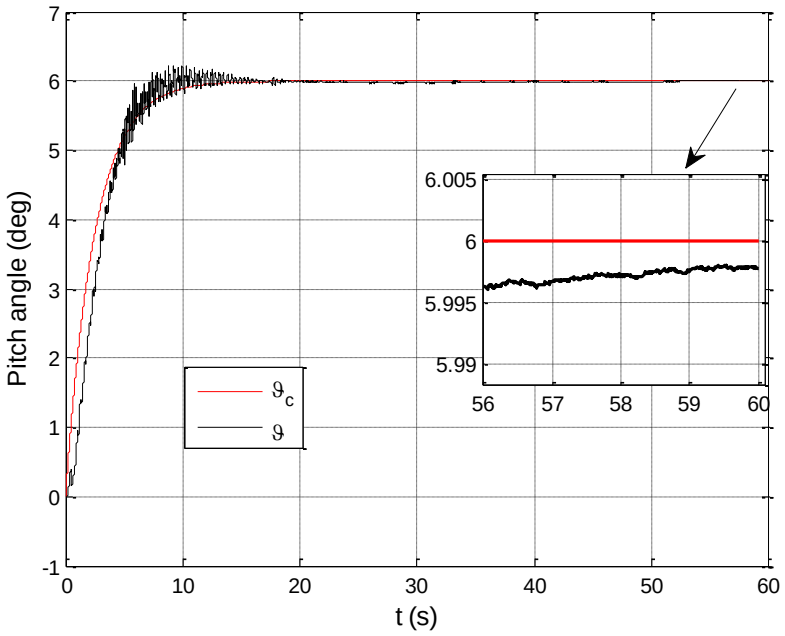

Fig. 5 Pitch angle response.

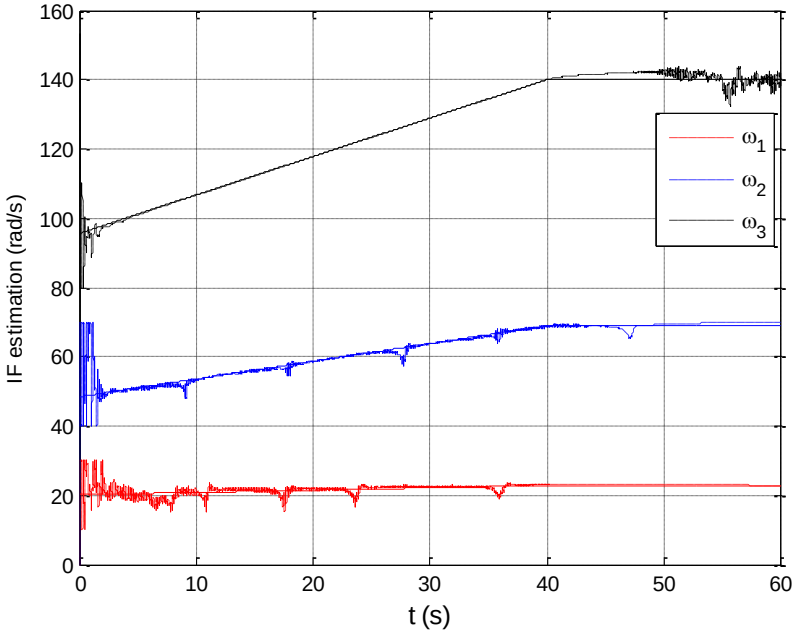

Fig. 6 Instantaneous frequency estimations.

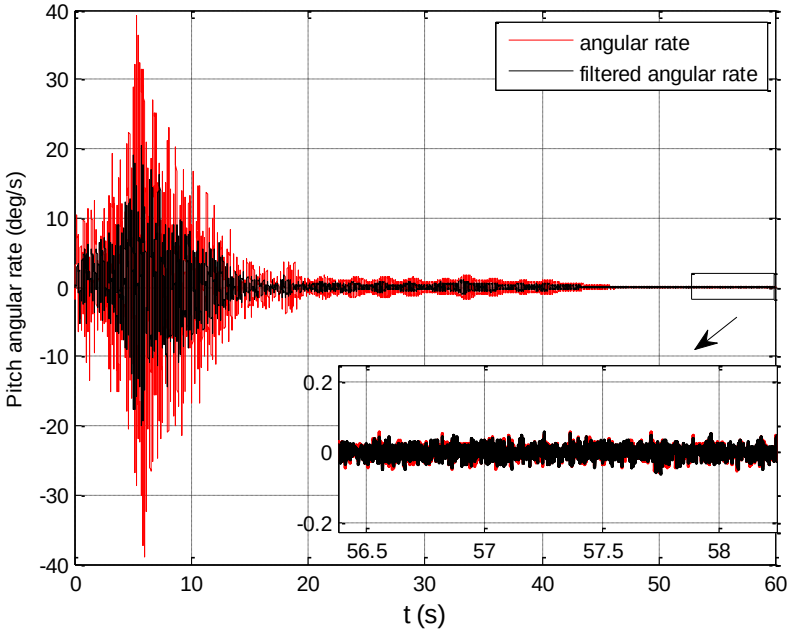

Fig.7 Measurement of angular velocity and the output of the ANF.

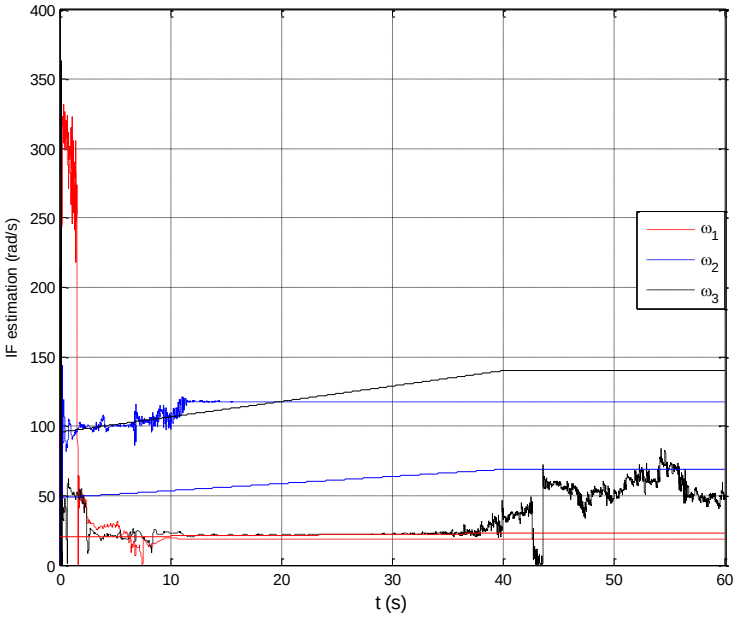

Fig. 8 Instantaneous frequency estimations.

6. Conclusions

In this paper, we investigated a practical adaptive notch filter design approach for the aeroservoelasticity suppression of the flexible high-speed vehicle. Direct frequency estimation scheme is employed since the online frequency monitoring is necessary for practical application and the indirect frequency estimation method is computationally complicated and sensitive to the polynomial coefficients. Two structures for the realization of the direct frequency estimation, the IA and SA, are compared. A strategy based on the priori knowledge about the frequency range is proposed to supervise the frequency estimation and enhance the convergence performance of the IA and SA. The estimation bias of the supervised SA (SSA) scheme is found to be smaller than that of the supervised IA (SIA) both in tracking the stationary and time-varying frequencies. Thus, the SSA method is more favourable

in practice due to the high precision and robustness. At last, simulations on a flexible high-speed vehicle to simultaneously suppress three structural modes are performed to demonstrate the effectiveness of the proposed SSA.

Reference

1. Piao M, Zhang Y, Sun M, et al. Adaptive aeroservoelastic mode stabilization of flexible airbreathing hypersonic vehicle[J]. Journal of Vibration and Control, 2019, 25(15): 2124-2142.
2. Levin J, Ioannou P and Mirmirani M. Adaptive mode suppression scheme for an aeroelastic airbreathing hypersonic cruise vehicle[C]. In: AIAA Guidance, Navigation and Control Conference and Exhibit, Hawaii, USA, AIAA 2008-7137.
3. Pei S, Tseng C. A novel structure for cascade form adaptive notch filters[J]. Signal Processing, 1993, 33(1): 95-110.
4. Chen B, Yang T, Lin B, et al. Adaptive notch filter by direct frequency estimation[J]. Signal Processing, 1992, 27(2): 161-176.
5. Li G. A stable and efficient adaptive notch filter for direct frequency estimation[J]. IEEE Transactions on Signal Processing, 1997, 45(8): 2001-2009.
6. Fiorentini L. Nonlinear adaptive controller for air-breathing hypersonic vehicles. PhD Thesis, The Ohio State University, Columbus, USA, 2010.
7. Han J. From PID to active disturbance rejection control[J]. IEEE Transactions on Industrial Electronics, 2009, 56(3): 900-906.
8. Piao M, Yang Z, Sun M, et al. A practical attitude control scheme for hypersonic vehicle based on disturbance observer[J]. Journal of Aerospace Engineering, Proceedings of the Institution of Mechanical Engineers Part G, 2019, 233(12): 4523-4540.
9. Nehorai A. A minimal parameter adaptive notch filter with constrained poles and zeros[J]. IEEE Transactions on Acoustics, Speech, and Signal Processing, 1985, 33(4): 983-996.
10. Ng T, Chicharo J F. IIR notch filtering-comparisons of four adaptive algorithms for frequency estimation[C]. International symposium on circuits and systems, 1995: 865-868.
11. Ng T. Some aspects of an adaptive digital notch filter with constrained poles and zeros[J]. IEEE Transactions on Acoustics, Speech, and Signal Processing, 1987, 35(2): 158-161.
12. Boashash B. Estimating and interpreting the instantaneous frequency of a signal-part 2: Algorithms and applications. Proceedings of the IEEE, 1992, 80(4): 540–568.